Determining the mechanical constitutive properties of metals as a function of strain rate and temperature: A combined experimental and modeling approach

Final Report

PI. Ian Robertson

Co-PI. John Lambros
Co-PI. Armand Beaudoin

`

Project Summary: Development and validation of constitutive models for polycrystalline materials subjected to high strain-rate loading over a range of temperatures are needed to predict the response of engineering materials to in-service type conditions. To account accurately for the complex effects that can occur during extreme and variable loading conditions, requires significant and detailed computational and modeling efforts. These efforts must be integrated fully with precise and targeted experimental measurements that not only verify the predictions of the models, but also provide input about the fundamental processes responsible for the macroscopic response. Achieving this coupling between modeling and experiment is the guiding principle of this program. Specifically, this program seeks to bridge the length scale between discrete dislocation interactions with grain boundaries and continuum models for polycrystalline plasticity. Achieving this goal requires incorporating these complex dislocation–interface interactions into the well-defined behavior of single crystals. Despite the widespread study of metal plasticity, this aspect is not well understood for simple loading conditions, let alone extreme ones.

Our experimental approach includes determining the high-strain rate response as a function of strain and temperature with post-mortem characterization of the microstructure, quasi-static testing of pre-deformed material, and direct observation of the dislocation behavior during reloading by using the *in situ* transmission electron microscope deformation technique. These experiments will provide the basis for development and validation of physically-based constitutive models. One aspect of the program involves the direct observation of specific mechanisms of micro-plasticity, as these indicate the boundary value problem that should be addressed. This focus on the pre-yield region in the quasi-static effort (the elasto-plastic transition) is also a tractable one from an experimental and modeling viewpoint. In addition, our approach will minimize the need to fit model parameters to experimental data to obtain convergence. These are critical steps to reach the primary objective of simulating and modeling material performance under extreme loading conditions.

During this project, the following achievements have been obtained:

1. Twins have been observed to act as barriers to dislocation propagation and as sources of and sinks to dislocations.
2. Nucleation of deformation twins in nitrogen strengthened steel is observed to be closely associated with planar slip bands. The appearance of long twins through heavily dislocated microstructures occurs by short twins nucleating at one slip band, propagating through the dislocation-free region, and terminating at the next slip band. This process is repeated throughout the entire grain.
3. A tamped-laser ablation loading technique has been developed to introduce high strain rate, high stress and low strains.
4. Both dislocation slip and twinning are present in high strain-rate deformed zirconium, with the relative contribution of each mode to the deformation depending on the initial texture.
5. *In situ* IR thermal measurements have been used to show that the majority of plastic work is dissipated as heat even under conditions in which twinning is the dominant deformation mode.

Table 1. Project participants, Affiliations and Percentage of time supported by this grant.

Principal Investigators	Department Affiliation	Fraction of time supported by this grant
Professor I. Robertson	Materials Science and Engineering (MatSE)	0.5 month
Professor A. Beaudoin	Mechanical Science and Engineering (MechSE)	1 month
Professor John Lambros	Aerospace Engineering (AE)	1 month
Graduate Students		
Cindy Smith	MatSE	100 %
Bryan Miller	MatSE	100 %
Jamie Kimberley	AE	100%
Henry Padilla	MechSE	100 %
Satya Varadhan	MechSE	100 %
Collaborators at National Laboratories		
Jeff Colvin	LLNL	
Geoff Campbell	LLNL	
Paul de Mange	LLNL	
Carlos Tomé	LANL	
George Kaschner	LANL	
Dave Korzekwa	LANL	
Brain Somerday	SNL	

The focus of our program has been the characterization of the competition between slip and twinning deformation modes in HCP and FCC metals with an emphasis on evaluating the hardening effect of twins. There are three aspects to the program: bulk mechanical property assessment, microstructure characterization, and modeling. In each aspect multiple approaches are employed. The mechanical behavior is probed using quasi-static compression tests on a servo-hydraulic load frame, interrupted strain dynamic compression tests via the split-Hopkinson pressure bar (SHPB) and a newly developed laser-loading technique. Characterization of the deformation structure utilizes several techniques to probe the evolution of texture and deformation mode with strain. Interrupted tests provide snapshots in the strain history of the evolving microstructure and serve as the starting material for *in situ* straining experiments in the transmission electron microscope. This latter technique allows the evolution of the microstructure to be directly observed as a function of strain.

Behavior of FCC Materials

The work with FCC materials during this project has focused on two areas related to the impact of twin boundaries on deformation behavior. These areas are: the ability of twin

boundaries to act as barriers to dislocation slip, and the transition in deformation mode from dislocation slip to deformation twinning as a function of strain and strain rate. For the former area of study, efforts focused on experimentally measuring the strength of twin boundaries to determine a relation between boundary strength and misorientation. These experiments used nano-indentation to quantify boundary "strength". In addition to this approach, *in situ* TEM deformation experiments were used to observe and characterize the defect structure produced during slip transmission across a coherent annealing twin boundary. This approach is found to be a more useful technique than nano-indentation for observing the details of the complex interactions between dislocations and coherent twin boundaries.

In FCC materials, deformation occurs primarily by dislocation slip, however, when deformed at low temperature and/or high strain rate, deformation twinning becomes a much more active mechanism. The propensity for deformation twinning increases for FCC materials with low stacking-fault energy and large grain size. Several outstanding issues related to the change in deformation mode have been addressed in this project. Specifically, efforts have focused on identifying the mechanism responsible for the nucleation and propagation of deformation twins as a function of strain and strain rate. For deformation at elevated strain rate, the tamped-laser ablation technique was employed to achieve deformation at low levels of strain but at strain rates up to 10^6 s^{-1}. This has enabled the characterization of defect structures prior to the onset of deformation twinning.

Slip Transmissibility from Twin Boundaries

Knowing the dependence of grain boundary strength, also referred to as the slip transmissibility factor, as a function of grain boundary misorientation is a key parameter required for advancing the development of plasticity models that incorporate grain boundary effects. As reported in the 2004 Progress Report, nano-indentation experiments were used to measure the hardness of a grain boundary and the region vicinal to it in an effort to quantify the "strength" of the boundary, and subsequently, how resistant a particular type of boundary is to slip transmission.

Several types of grain boundaries in copper produced by different mechanical treatments were examined. In general, twin boundaries and high angle boundaries in annealed copper yielded hardness values between 2.1 and 2.5 GPa. In an as-received sample of copper, grain boundary hardness was measured to be 3.77 GPa. This higher value is attributed to the underlying dislocation microstructure, which was typical of a worked metal. Because of the close range in hardness values measured for twin boundaries and high angle grain boundaries, it is difficult to relate the hardness as determined by nano-indentation and, hence the slip transmissibility factor, and grain boundary misorientation.

To better understand slip transmissibility across grain boundaries in the nano-indented samples, we proposed (in the 2004 Progress Report) to use a Focused Ion Beam (FIB) machine to prepare TEM samples from the indented regions. This would allow for the direct observation and characterization of the defect structure generated from the grain boundary after indentation and for the accurate determination of the grain boundary misorientation. Despite numerous attempts, we were unable to prepare a sample of sufficient quality to observe the defect structure. Because of this, the use of nano-indentation was discontinued in favor of the *in situ* TEM deformation experiments.

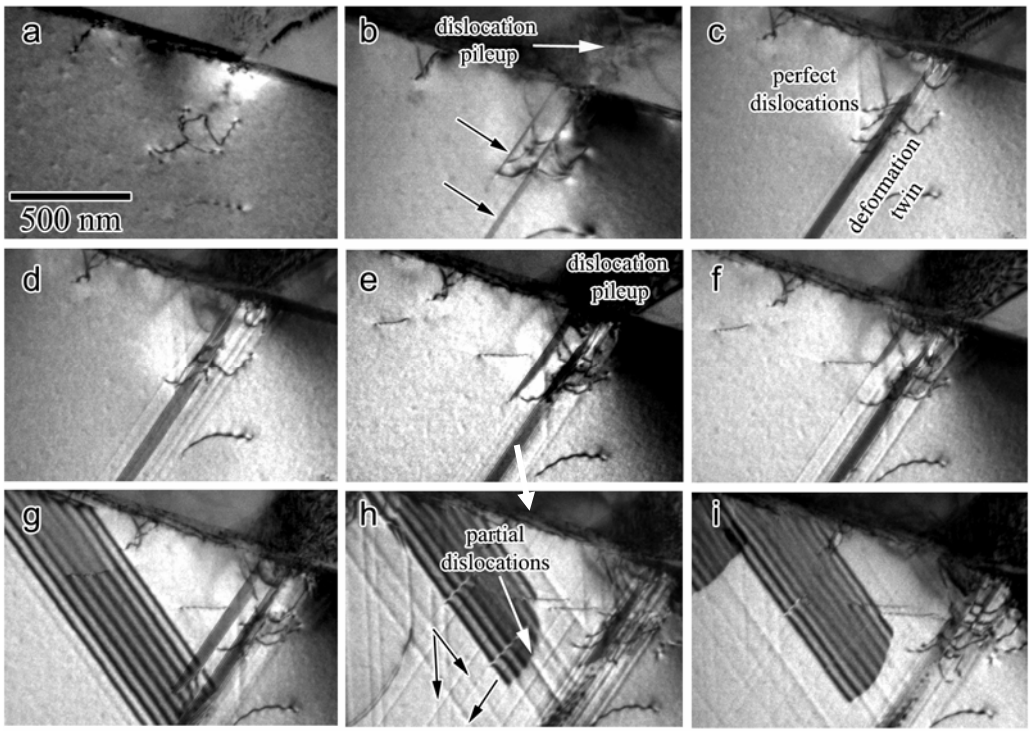

Figure 1. Image sequence showing activation of multiple slip systems from a coherent twin boundary. Perfect and partial dislocations as wells as a deformation twin are produced by the twin boundary in response to the applied and local stress condition.

The *in situ* TEM deformation technique allows for real-time observation of key deformation processes. This technique, coupled with standard TEM characterization of the resulting dislocation structures and misorientation between grains, provides more information for determining the effects of local stress concentrations on slip transmissibility for any type of grain boundary. Room temperature, *in situ* TEM deformation experiments performed during this project focused on slip transmission across coherent twin boundaries in a solution-strengthened Cu-4wt%Al alloy. This alloy has a low stacking fault-energy and was annealed to produce a large grain size with a high density of annealing twins prior to *in situ* deformation.

An example of slip transmission across a twin boundary is shown in the sequence of images presented in Figure 1. The dislocation pileup responsible for producing a high local stress is indicated in Figure 1b. This stress must be superimposed on the applied stress. It is this combined stress will determine the slip systems activated by the twin boundary. It has been shown in prior work that the slip system activated is determined by competition between the local stress distribution and minimization of the strain energy in the grain boundary [1,2]. In this case, both perfect and partial dislocations are emitted from multiple sources along the boundary. Consequently, a complex microstructure evolves that includes the formation of a deformation twin, labeled in Figure 1c, and a density of partial and perfect dislocations. The deformation twin serves as a barrier to the perfect and partial dislocations as shown in the sequence of images presented in Figure 2. Perfect dislocations pileup at the deformation twin and are incorporated into the twin plane. This incorporation can be seen from the increase in the density of dislocations accumulated in the interface; Figure 2d shows several examples. The progress of the partial dislocations is also impeded by the twin boundary. The extended partial dislocation seen in Figure 1c approaches but never penetrates the twin boundary. With increasing dislocations

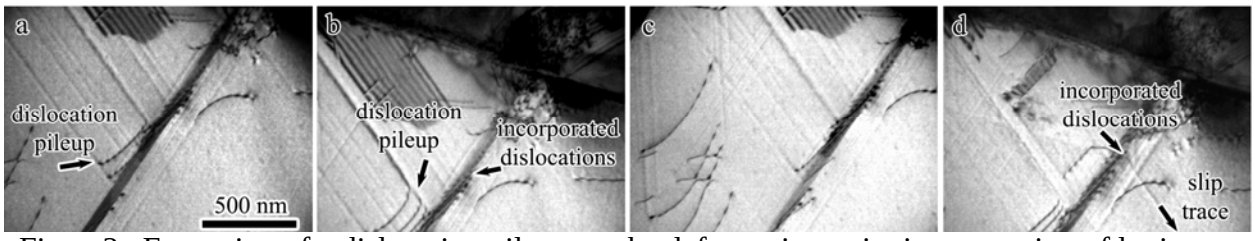

Figure2. Formation of a dislocation pile-up at the deformation twin, incorporation of lattice dislocations into the twin and eventually slip transmission.

activity, this stacking fault is subdivided and a new structure is formed; compare Figure 1c with Figures 2b and 2d. As evidenced by the lack of slip traces on the other side of the deformation twin, it is clear no slip transmission across it has occurred. As more dislocations are incorporated into the deformation twin and a dislocation pileup develops, the local stress level increases and eventually, as evidenced by the appearance of slip traces in Figure 2d, arrowed line, dislocations are ejected from the deformation twin and the process of slip transfer is initiated

To better understand the dislocation—twin boundary interactions, a collaboration with Dr. Jaime Marian at LLNL was initiated. Dr. Marian specializes in dislocation dynamics simulations. This collaboration offers the opportunity for Dr. Marian to simulate dislocation-twin boundary interactions, something that has previously proved difficult due to lack of data on how twin boundaries respond to high levels of local stress. The results of these simulations will provide us with a better understanding of the dislocation accommodation mechanisms in the twin boundary and how dislocation sources are activated within the twin boundary.

The Onset of Deformation Twinning as a Function of Strain and Strain Rate

A major goal of this project has been to develop an understanding of the fundamental processes that occur during high strain-rate deformation. In particular, the underlying mechanisms responsible for the change in deformation mode from dislocation slip to deformation twinning are of interest. Deformation techniques such the SHPB and tamped-laser ablation have been employed to deform low stacking-fault energy face-centered cubic materials at high strain-rate. The resulting defect structure has been examined using conventional TEM characterization techniques.

One challenge in identifying deformation mechanisms operating in high strain-rate deformed materials is the high defect density, which can obscure identification of controlling mechanisms. This is illustrated in the micrographs presented in Figure 3 which show the defect structures present in two different grains of a Cu-4wt%Al alloy deformed in compression at room temperature at a strain rate of 10^3 s^{-1}. This sample has been deformed to 12% true strain. A dense defect structure consisting of dislocations on multiple slip systems and deformation twins has been produced. The density of defects present makes it difficult to determine the twin nucleation and propagation mechanisms. For instance, the deformation twins are observed to propagate large distances in a grain containing a high density of defects. This raises the question of how the partial dislocations at the leading edge of the growing deformation twin interact with and break through the pre-existing dislocations. Further, it is interesting to note that deformation in one grain is dominated by dislocation slip while deformation twinning is the dominant mode of deformation in a nearby grain.

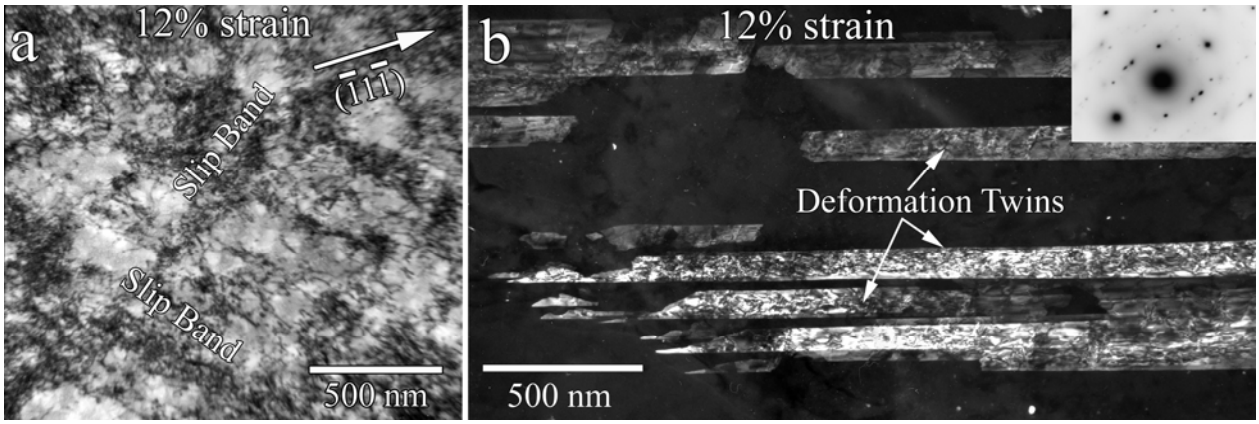

Figure 3. (a) Defect densities present in high strain-rate deformed Cu-4wt%Al after deformation to 12% strain. A change in deformation mode from dislocation slip to deformation twinning is evident in certain grains (b).

A drawback to the SHPB is the difficulty in interrupting the tests at different levels of strain to determine the evolution of the defect structure. In order to exert more control over interrupted strain tests, room temperature, quasi-static compression tests (strain rate of 10^{-3} s^{-1}) on a nitrogen-strengthened austenitic steel alloy, 21Cr-6Ni-9Mn have been conducted; this work was performed in collaboration with Dr. Brian Somerday of Sandia National Laboratory.

As shown in Figure 4, the steel exhibits the same transition in deformation mode from dislocation slip to deformation twinning that is observed in the room temperature SHPB tests on Cu-4wt%Al. In the sample deformed to 5% strain (Figure 4a) deformation occurs by slip of perfect and partial dislocations. Development of planar slip bands due to a lack of cross-slip is evident. With increasing strain, ~35%, deformation twins are found interspersed within a high density of dislocations; see Figure 4b. The presence of twins is confirmed by the electron diffraction pattern shown in the inset in Figure 4b.

At ~10% strain the planar slip bands become more pronounced and, as shown in Figure 5a, complex dislocation structures consisting of partial dislocations connected by stacking-fault

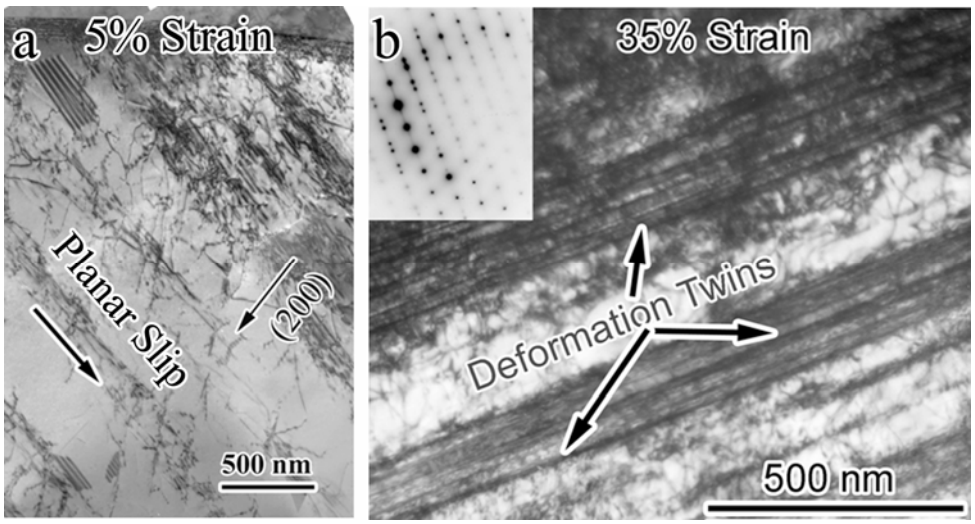

Figure 4. Comparison of defect structure present in nitrogen-strengthened stainless steel deformed to (a) 5% strain and (b) 35% strain.

`

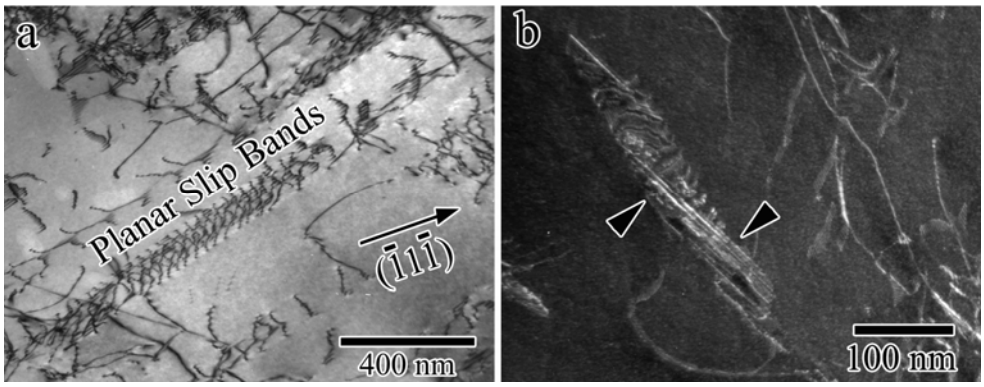

Figure 5. a) deformation structure after 10% strain. b) development of twin embryo inside the deformation band. This image was formed with a twin diffraction spot.

ribbons are developed within the slip band. This suggests the local stress has reached a level where it can no longer be accommodated solely by slip of perfect dislocations. Because cross-slip is suppressed, twins are generated from within the slip band; the specific nucleation site and mechanism were not identified in the current work. The formation of a twin embryo is seen in Figure 5b; the indicated feature in this image, which was formed with a twin diffraction spot, is the nucleus

With increasing strain, large numbers of deformation twins are seen to nucleate from individual planar slip bands. Figure 6a shows a bright-field image of an array of twins emanating from and stopping at a slip band. Agglomeration of these short segmented twins results in the formation of a twin that appears to extend completely through a grain. Evidence that these extended twins are composed of smaller segments can be seen in Figure 6b, in which steps, marked by arrowheads, are found in long twins. The separation distance between the arrows is consistent with the distance between the slip bands. These observations present a possible explanation of the formation of grain-spanning twins through a dense field of pre-existing dislocations.

The results of the quasi-static tests suggest that deformation twins in the high-nitrogen steel are nucleated as a means to accommodate high local stresses developed from dislocation

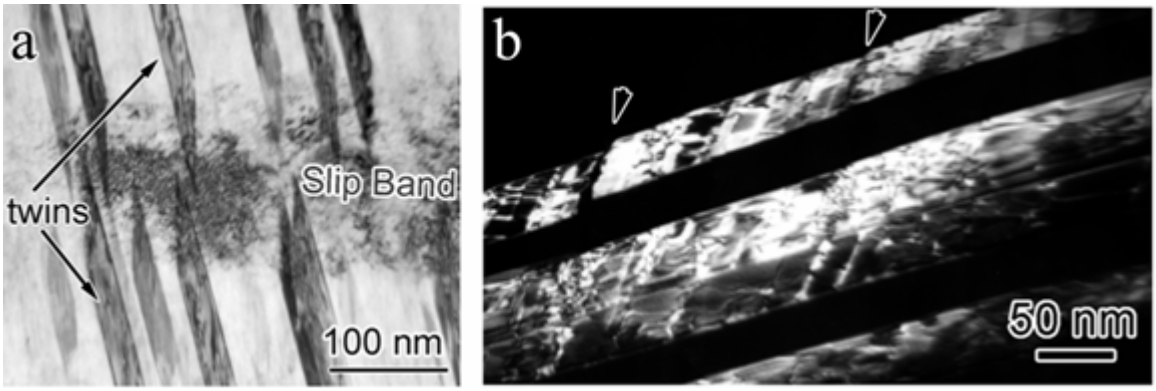

Figure 6. (a) Numerous deformation twins are seen to nucleate from planar slip bands with increasing strain. (b) Long bands of deformation twins are observed to form from the overlap of the short twin segments formed between planar slip bands. The arrowheads in (b) denote discontinuities where the twin segments overlap.

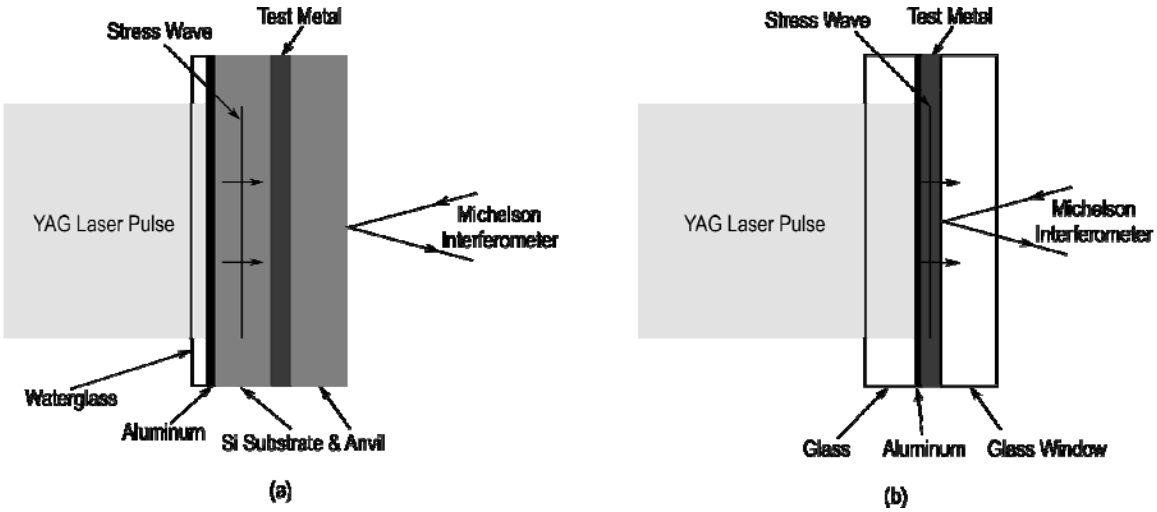

Figure 7. Schematic showing the (a) original laser loading specimen design, and (b) the tamped ablation configuration.

interactions in planar slip bands. Extending these observations to account for deformation twins that nucleate during high strain-rate deformation is difficult as the pre-existing defect structure produced during deformation masks the twin nucleation mechanism. The observations are also hindered by the difficulty in interrupting SHPB tests at specific levels of strain to observe the evolution of the defect structure (see Figure 3). To overcome these shortcomings, a laser-based loading technique that would allow for high strain-rate deformation to low levels of strain was developed. The setup is similar to a flyer-plate test, but on a much smaller scale.

A schematic of the original set-up is shown in Figure 7a. A pulsed Nd:YAG laser (pulse energy 1 J, pulse duration 10 ns, wavelength 1064 nm) is focused to a 3 mm-diameter spot on the surface of a 5 mm-diameter, 500 μm-thick silicon wafer. This wafer was coated with an aluminum absorbing layer and a confining layer that is transparent to the YAG laser wavelength. Upon application of the laser pulse the aluminum is vaporized and undergoes a rapid volumetric expansion. The confining layer serves to trap this expansion thus launching a compressive stress pulse into the silicon wafer. This pulse travels through the wafer and is transmitted through the test metal and into the silicon wafer anvil, deforming the sample in the process. The free surface displacement of the rear surface of the anvil is monitored during the course of the experiment allowing for the stress in the test metal to be determined by means of one-dimensional wave propagation arguments. It was stated in the 2004 Progress Report that post-mortem TEM analysis of single crystal and polycrystalline copper deformed with this laser technique showed the presence of deformation twins. The low density of twins was a cause for concern and further studies revealed that these twins were in fact sample preparation artifacts. This necessitated a redesign of the experimental set-up to the tamped ablation configuration shown in Figure 7b. The removal of the substrate results in a larger pressure acting directly on the sample, and consequently an increase in the stress, 3 GPa vs. 0.5 MPa.

Initial findings from tamped-laser ablation deformed Cu-4wt%Al were presented in the 2005 Progress Report. These early findings suggested that mechanisms of deformation depended on the orientation of individual grains relative to the loading axis. Perfect dislocations on multiple slip systems existed in certain grains while other grains exhibited deformation by both perfect and partial dislocations. Examples of the defect structure are presented in Figure 8. In Figure 8a, perfect dislocations are seen arranged in planar slip bands on different slip planes in

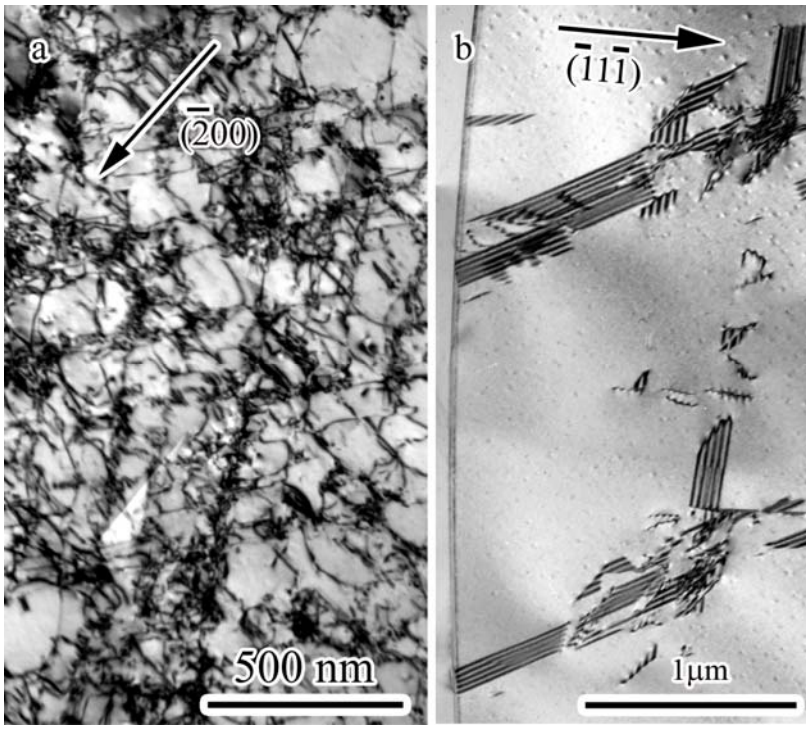

Figure 8. (a) Deformation occurs solely by slip of perfect dislocations in a grain with $\{011\}$ orientation and (b) by slip of partial dislocations in a grain with $\{112\}$ orientation. The difference in densities of defects present in each grain could result from the effects of constraints, such as grain boundaries, on the local stress states.

a grain orientated close to $\{011\}$. From the defect density present, it is clear that deformation to several percent strain occurred. In contrast, in Figure 8b, deformation occurs solely by partial dislocations acting on multiple slip systems in a grain orientated close to $\{112\}$. It is important to note that these results do not suggest that all grains with these orientations will exhibit a similar microstructure. Rather the suggestion is that in addition to the grain orientation the nature of the constraints imposed by the surrounding grains must be taken into consideration.

To determine the effect of local constraints on the stress distribution in a particular grain, the stress variations due to elastic anisotropy were calculated for actual grain misorientations. The misorientation map for an undeformed electropolished TEM foil is shown in Figure 9a and the corresponding stress distribution is shown in Figure 9b. Clearly, even with this simplified model, there is variation in the stress distribution due to the local constraints imposed by surrounding grains. This aspect of the program needs to be explored further.

A second factor that needs to be considered is the decay of the laser generated shock pulse as it traverses the sample. As such, the pressure of the shock pulse will vary with distance from the front surface of the sample and will likely affect the operative deformation mechanisms. The defect structures shown in Figure 8 are located in a region of unknown depth from the front surface. Due to the sample preparation techniques for TEM, it is not possible to accurately control the depth within the sample where the electron transparent region is formed. Thus, it is currently not possible to quantify the relationship between the actual stress level in a grain and deformation modes observable in the TEM.

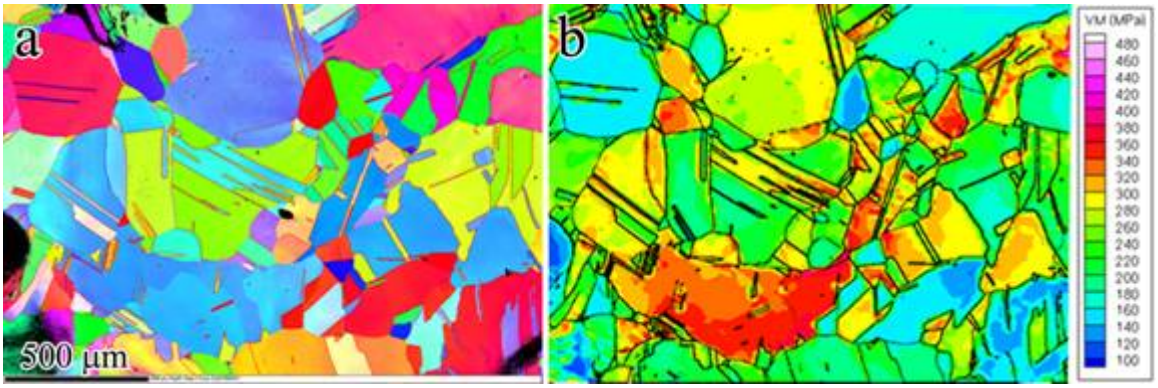

Figure 9. (a) EBSD grain orientation map of an undeformed electropolished TEM foil of Cu-4wt%Al. (b) Contours of von Mises stress illustrating the effect of elastic anisotropy on the stress distribution.

To relate the effects of the shock pulse to the deformation mechanisms, collaborations with Drs. Geoff Campbell, Jeff Colvin, and Paul DeMange at LLNL were initiated. The goal of this effort is to simulate the response of the laser deformation experiments using the 1-D hydrocode HYADES. With this code the initial pressure of the shock pulse at the front surface of the sample material can be calculated. This quantity is not accessible experimentally. Furthermore, the simulation results will predict the pressure decay of the shock pulse as a function of distance traveled from the surface. This information should be correlated with the depth dependence of the defect structure. The simulations developed in this effort will provide a tool to study how changes in the experimental setup can be used to optimize the shock pulse produced within the sample material.

Behavior of an HCP Material

The lack of abundant slip systems in HCP metals plays an important role in determining how slip and twinning account for the plastic deformation. To better understand the deformation mechanisms important to low-symmetry metals, the mechanical and thermomechanical response of polycrystalline zirconium was studied under compressive loading in a SHPB at strain rates on the order of 10^3 s^{-1}. Optical microscopy, static TEM, and bulk x-ray diffraction (XRD) texture measurements were performed on undeformed and deformed specimens. These techniques showed that uniaxial compression along the bar axis produced both deformation twins and dislocation activity. Further progress in this area was made by studying effects of plate orientation for a rolled plate of commercially pure zirconium (grade 702). These results are published as Padilla *et al.* [3]. For this material, the relationships between mechanical response, texture, microstructure, and dissipation of plastic work are complemented by simulation using the visco-plastic self-consistent (VPSC) code developed at Los Alamos National Laboratory (LANL) [4,5]. Drs. Carlos Tomé and George Kaschner of LANL have participated in several discussions related to material selection, mechanical testing, analysis of results, and implementation of the VPSC modeling. In addition, Dr. Kaschner serves on the Dissertation Committee for Henry Padilla.

As outlined here and detailed in the annual report for 2005, the experimental procedure for studying the thermomechanical response to high strain-rate loading involved coupling a SHPB setup for compression with a high speed infrared detector array. The latter enables the

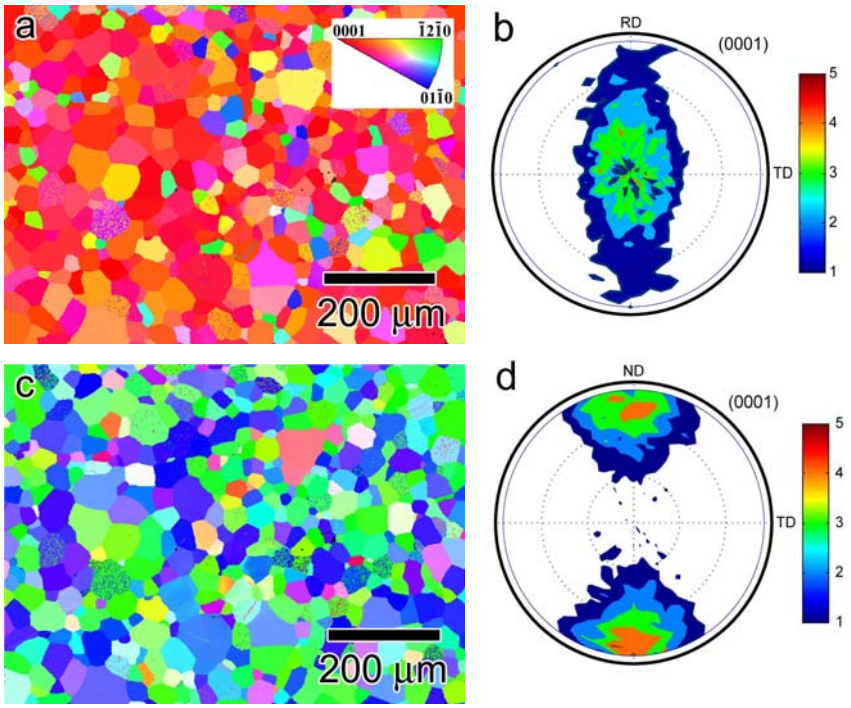

Figure 10. Undeformed texture measurements of rolled zirconium plate. (a) EBSD grain orientation map and a (b) (0001) x-ray diffraction pole figure, both measured along the plate normal direction. (c) EBSD grain orientation map and a (d) (0001) x-ray diffraction pole figure, measured along the plate rolling direction. ND favors basal orientations, while RD favors non-basal orientations.

sample temperature to be monitored. From this it is possible to determine the fraction of plastic work dissipated as heat.

EBSD and x-ray diffraction measurements, shown in Figure 10, demonstrate that specimens cut along the through-thickness (Figure 10a) and in-plane rolling (Figure 10b) plate directions have a strong basal and non-basal texture, respectively. This initial texture is similar to the clock-rolled zirconium texture processed at LANL [6,7] with regard to the predominant alignment of the basal pole near the plate normal direction, although the variation in the rolled plate is somewhat greater.

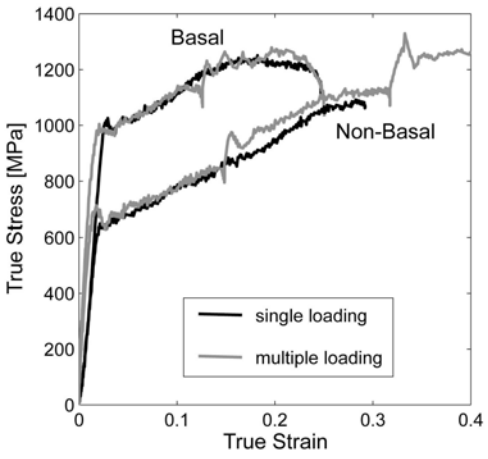

Figure 11. True stress vs. true strain response for basal and non-basal textured zirconium.

With these starting textures, two distinct types of mechanical response were observed in both single- and multiple-loading experiments. For the latter tests, longer specimens are loaded once, re-lubricated, and loaded a second time at a similar strain rate to achieve larger strains. Figure 11 shows that basal oriented specimens have a much higher yield and flow stress than the non-basal specimens, as well as having lower ductility. Clock-rolled higher purity zirconium studied by Kaschner *et al*. [6] has lower yield and flow stress

`

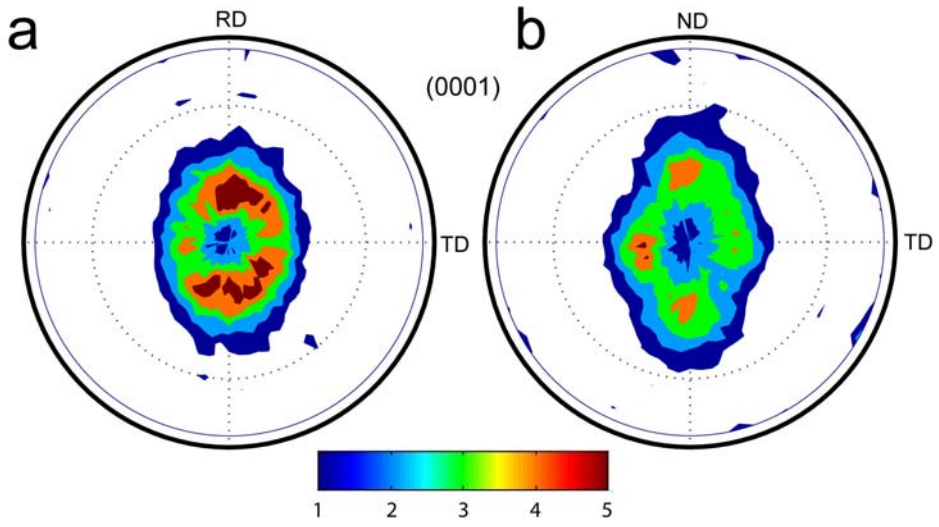

Figure 12. XRD texture measurements of deformed zirconium specimens. (a) Basal textured specimen compressed to 20% strain. (b) Non-basal texture specimen compressed to 40% strain.

but a similar trend between basal and non-basal textures, with the difference that some of the clock-rolled data is collected at test temperatures of 77K and at a strain rate of 10^{-3} s^{-1}.

Bulk XRD texture measurements of deformed specimens show a drastic difference between basal and non-basal oriented specimens. A basal textured specimen (example shown in Figure 12a) shows less spread in texture after 20% strain, but no major changes in peak locations (compare to Figure 10b), whereas a non-basal specimen (Figure 12b) shows a drastic shift in (0001) peak intensity (compare to Figure 10d). To interpret these results, knowledge of the relevant deformation mechanisms and how they impact the texture is needed. The possible slip and twinning mechanisms are shown schematically in Figure 13. The observed texture changes are caused by significant deformation twinning, which causes sudden texture shifts by discrete

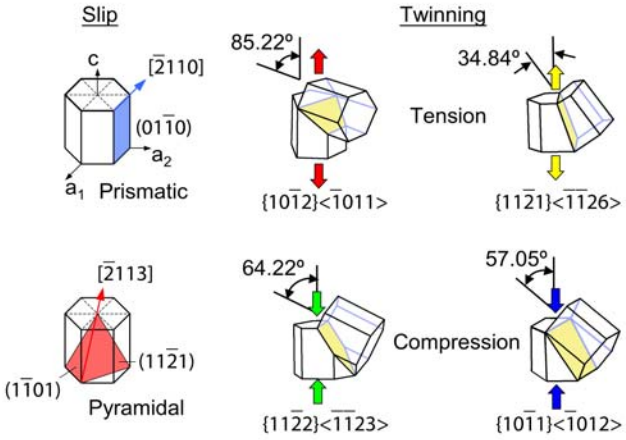

Figure 13. Schematic of slip and twinning mechanisms which may activate during plastic deformation of HCP metals.

`

amounts associated with the crystallographic reorientations indicated in Figure 13. Post-mortem electron microscopy showed the density of compression twins to be greatest in basal-textured samples, whereas tensile twins dominated non-basal textured samples. Examples of the deformation microstructure are presented in Figure 14. Both dislocations and twins are present in deformed specimens with basal and non-basal initial textures. Two types of tension twins (Figure 13) were observed in both the basal and non-basal textured samples, although the twin density was higher in the non-basal textured sample. At this length scale, however, it is difficult to ascertain the level of activity of the twinning mechanisms quantitatively. The non-basal textured specimens, however, do display second generation twins, as indicated in Figure 14b. These twins are small and may not be resolved by other techniques (such as optical or SEM). The presence of both dislocations and second generation twins within a twin (Figure 14b) show that both deformation mechanisms are active and important even within already twinned regions.

The specific mode of deformation twinning can be identified using the technique described by Mason [8]. Twin axis—angle relations for the four twin modes shown in Figure 13 are used to identify boundaries with the right crystallographic character from EBSD orientation maps like those shown in Figure 15. Subsequent examination of the misorientation across boundaries removes incorrectly identified boundaries (grain boundaries mistaken for twin boundaries). Table 2 lists the crystallographic data used to identify these boundaries. Also listed in Table 2 are the computed area fractions for each twin mode, grouped by initial texture of the specimen. The largest area fraction is found to be composed of $\{10\bar{1}2\}$ tensile twins. The density of tensile twins is greater than that of compression twins in the basal-textured sample. This agrees with the visual observation that deformation twins are found mostly in non-basal oriented grains, which means that there is enough shear stress projected on the K_1 planes of the tensile modes in these non-basal oriented grains to activate tensile twinning before compression twinning. After examining the mechanical response, textures and deformed microstructures, it is clear that different mechanisms are active in the basal and non-basal textured specimens, which contribute to different responses to high strain-rate loading.

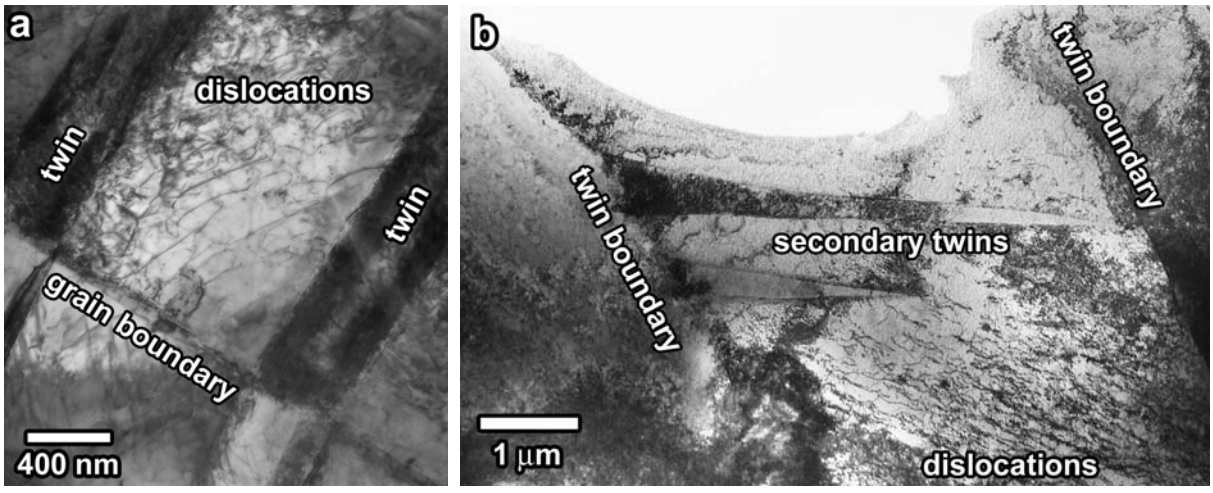

Figure 14. TEM images from (a) a sample with basal texture deformed at a strain rate of 1500 s-1 to 3.7.% strain and (b) a sample with non-basal texture deformed at a strain rate of 3700 s-1 to 30% strain.

`

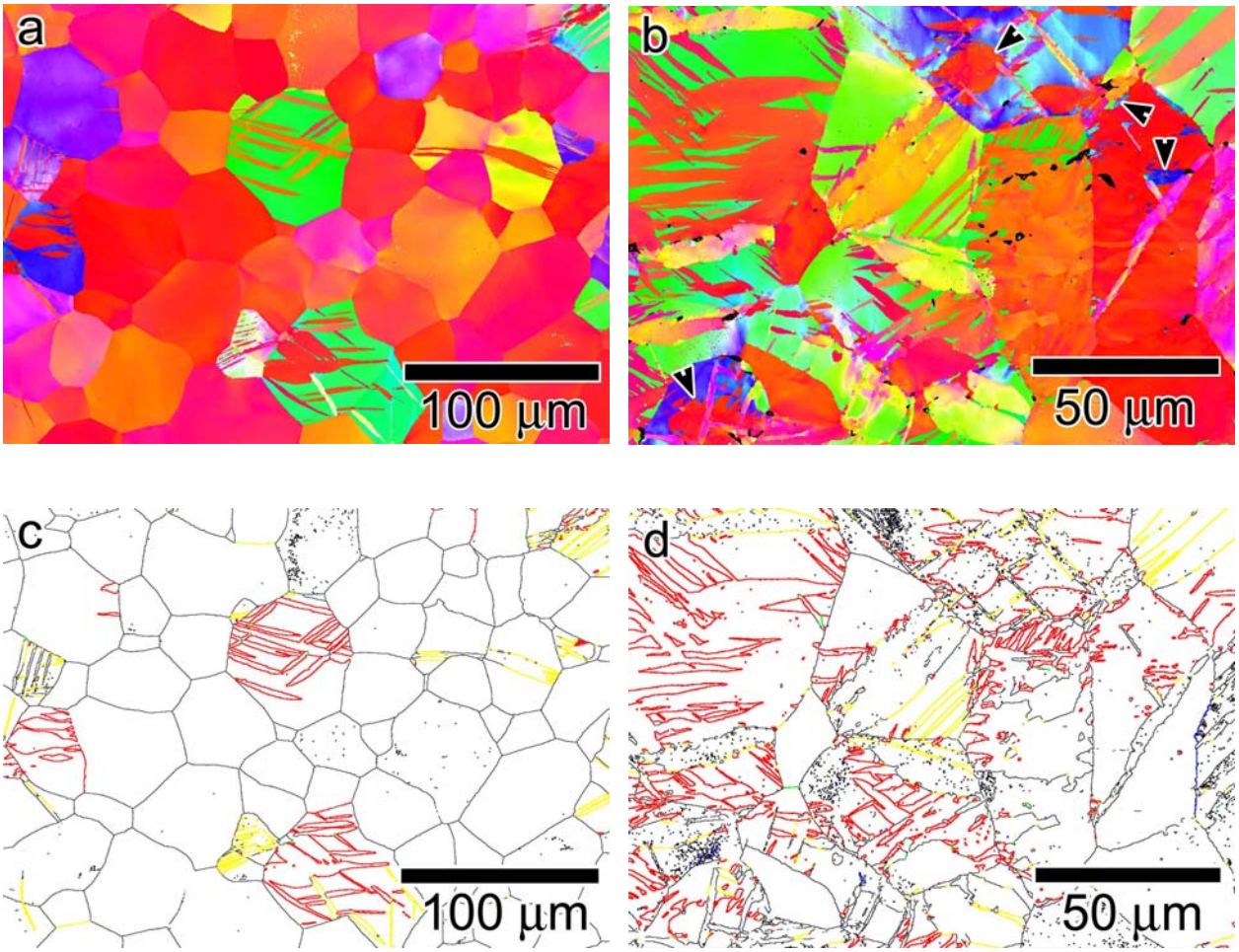

Figure 15. (a) Orientation map of basal textured sample deformed to 10% plastic strain. (b) Orientation map of non-basal textured sample deformed to 30% plastic strain. (c) Twin boundary analysis of deformed basal microstructure. (d) Twin boundary analysis of deformed non-basal microstructure. The colors in (c) and (d) refer to the four twin types listed in Table 2.

The change in texture in the non-basal orientated samples is likely due to the prominence of large $\{10\bar{1}2\}$ twins, which reorient the parent matrix by 85.2°. Deformation twins in the non-basal specimen are much more prevalent than in basal oriented specimens, implying that basal compression is largely accommodated by <c+a> pyramidal slip. The higher critical resolved shear stress of this system [9] would explain the larger yield and flow stress of basal-textured specimens.

`

					Area Fraction	
Type	K_1 Plane	η_1 Direction	Axis-Angle	TB Color	Basal	Non-Basal
T1	$\{10\bar{1}2\}$	$\{10\bar{1}\bar{1}\}$	$\langle 300\rangle$ - 85.2°	Red	4.6%	25%
T2	$\{11\bar{2}1\}$	$\{11\bar{2}\bar{6}\}$	$\langle 1\bar{1}0\rangle$ - 34.8°	yellow	2.2%	13%
C1	$\{11\bar{2}2\}$	$\{11\bar{2}3\}$	$\langle \bar{2}\bar{1}0\rangle$ - 64.2°	green	4.8%	-
C2	$\{10\bar{1}1\}$	$\{10\bar{1}\bar{2}\}$	$\langle 300\rangle$ - 57.1°	blue	-	1.0%
				Total	12%	39%

Table 2. Axis-angle relations and measured area fractions from twin boundary analysis of Figure 15

In terms of energy dissipation, the general consensus is that *most* materials dissipate 90% [10-12] or more of the plastic work as heat, with some evidence of incomplete dissipation in HCP metals [13]. It has been suggested that deformation twinning, which is common in these materials, may store this energy [11]. To assess this possibility the heat generated during the SHPB tests was measured and used to calculate the ratio between the heat dissipated and the plastic work done, β. This ratio can be described in differential form:

$$\beta_{diff} = \frac{\rho c_p \dot{T}}{\dot{W}^p} = \frac{\rho c_p \dot{T}}{\sigma \dot{\varepsilon}^p}, \tag{1}$$

and in integral form:

$$\beta_{int} = \frac{\rho c_p \left(T - T_o\right)}{\int_{\varepsilon_y}^{\varepsilon_f} \sigma d\varepsilon'}. \tag{2}$$

Thermal measurements (and the resulting β curves), which are generated using Equations (1) and (2) are shown in Figure 16. The results, shown in Figure 16 (c) and (d), demonstrate that less than 100% of the plastic work is dissipated as heat for a basal texture, whereas it is nearly 100% for a non-basal texture. As the non-basal textured sample shows the greater propensity for twinning, significant energy storage in twins does not happen. The basal-textured sample appears to show energy storage despite the fact that twinning is not the primary deformation mode. To understand this discrepancy, it is necessary to remember that the analysis is based on the assumption that the deformation is homogeneous. This is shown not to be a valid assumption as a shear band extending into the center of this specimen was found in a sample compressed to 22% plastic strain, see Figure 17. Thus, it can be concluded that the presence of twins does not provide a means of storing energy. These results show further that it is necessary to couple microstructural characterization to interpret correctly macroscopic property measurements in terms of microscopic processes.

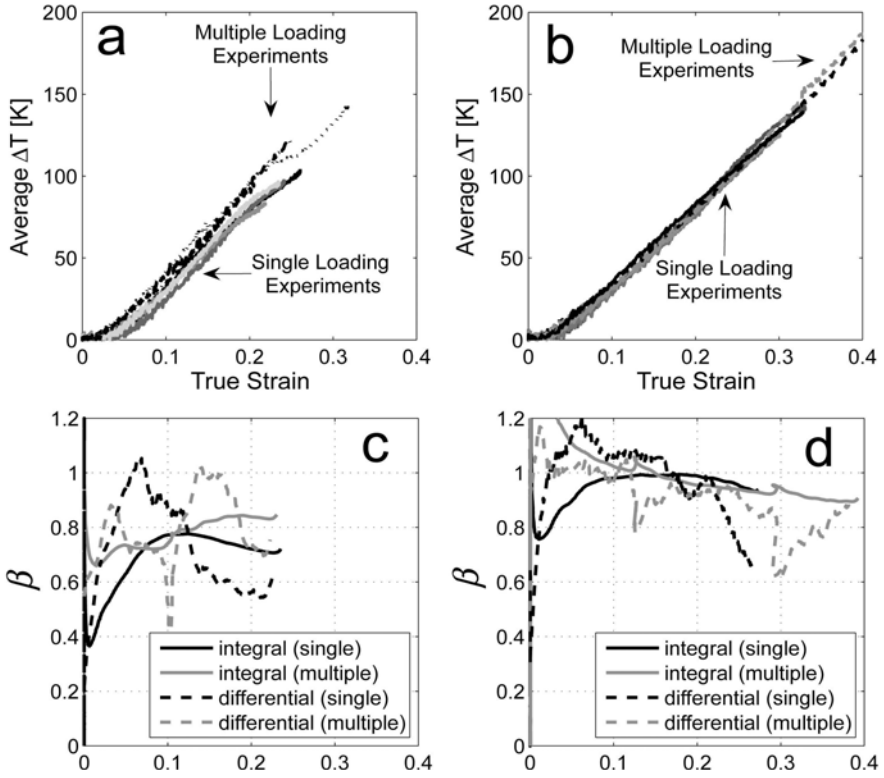

Figure 16. Average temperatures and computed *b* values are plotted *vs.* true strain for both single-loading specimens (solid lines) and multiple-loading specimens (dashed lines). Strain rates were all on the order of 10^3 s^{-1}. Results are displayed for several (a) basal textured and (b) non-basal textured specimens. Selected b_{int} and b_{diff} results which represent the overall trends are shown for (c) basal textured and (d) non-basal textured samples.

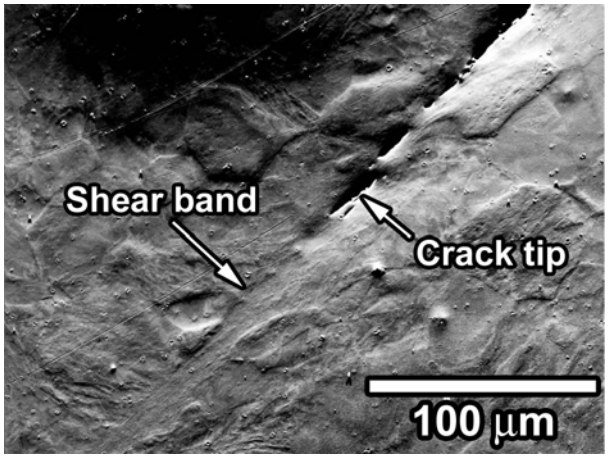

Figure 17. SEM micrograph of a sample with an initial basal texture. Specimen was deformed at a strain rate of 2500 s^{-1} to 22% plastic strain. Loading direction is oriented vertically in this image.

`

Modeling

To determine if the observed deformation modes were sufficient to account for the macroscopic stress-strain curves, the deformation was modeled by using the visco-plastic self-consistent code, which can account for the anisotropy of low symmetry materials [4,5]. Inputs to the code are: grain orientations, crystallographic definitions of available deformation mechanisms, and a Voce-type hardening law for each mechanism. An inverse method [14] that incorporates experimental stress-strain data, measured deformed textures, and comparison of active deformation mechanisms found using TEM and EBSD was used to determine hardening parameters for each deformation mechanism. The parameters which describe each hardening law are listed in Table 3. The mechanisms allowed in the simulation were $\{10\bar{1}0\}\langle 1\bar{2}10\rangle$ prismatic slip, which is the easiest mode to activate; $\{10\bar{1}2\}\langle\bar{1}011\rangle$ tensile twinning (T1); $\{11\bar{2}1\}\langle\bar{1}\bar{1}26\rangle$ tensile twinning (T2); and $\{10\bar{1}1\}\langle\bar{2}113\rangle$ pyramidal slip. The <c+a> pyramidal slip system is needed to accommodate c-axis compression for grains which grow large $\{10\bar{1}2\}$ tensile twins, and lie aligned with the loading axis. In addition, the basal-textured specimens demonstrate minimal compression twin formation, which is the only other means of accommodating c-axis compression.

Table 3. Hardening parameters for VPSC simulations of non-basal compression of zirconium. T1 and T2 are the first and second tension twinning modes shown in Figure 13.

Mode	Reference Threshold Stress [MPa]	Asymptotic Threshold Stress [MPa]	Reference Hardening Rate [MPa]	Asympotic Hardening Rate [MPa]	Latent Hardening (pyramidal)	Latent Hardening (prismatic)	Latent Hardening (T1)	Latent Hardening (T2)
Prismatic	60	60	2500	25	1	1	10	2
Pyramidal	250	75	200	160	1	1	2	2
$\{10\bar{1}2\}$ (T1)	130	130	100	15	1	1	10	10
$\{11\bar{2}1\}$ (T2)	230	230	125	100	1	1	10	10

Simulations were run in strain increments of 0.2% strain to 40% strain for comparison with deformed textures. The starting texture of the aggregate of grains was composed of 500 orientations, chosen from the non-basal texture measured by using EBSD scans, Figure 10. These orientations approximate an 8x8x8 aggregate of non-basal textured grains. The results of the simulation are shown in Figure 18. It is clear from the stress—strain response that the behavior is well predicted by the code with these parameters. Figure 18b shows a plot of the evolution of accumulated twin fraction, which, at the end of 30% strain, shows levels comparable to the area fraction measured from the non-basal compression sample. The relative shear contributed by each mechanism is shown in Figure 18c, and indicates that prismatic slip accommodates a large percentage of the shear in the aggregate. In the project review for 2005, similar simulations were discussed that pertained to the higher purity clock-rolled material used by collaborators at LANL. One of the differences between the two simulations is the type of

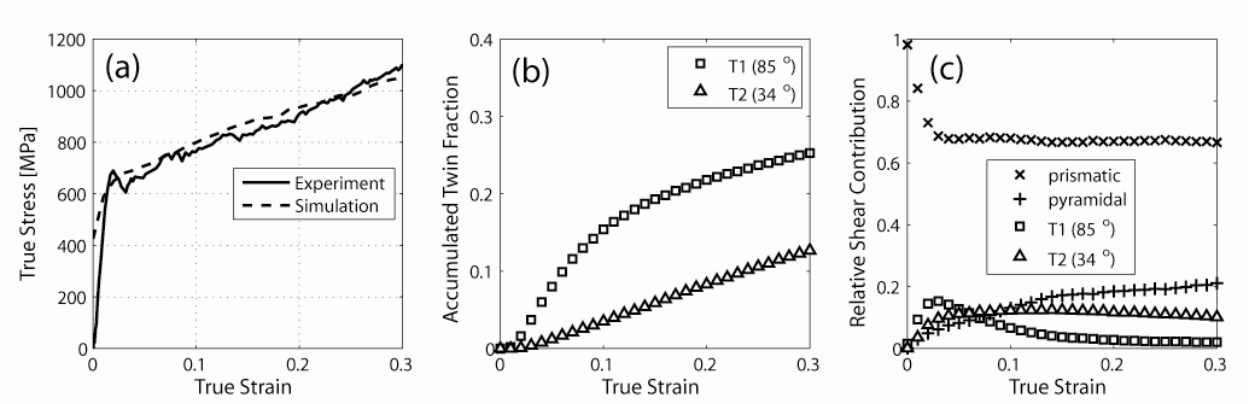

Figure 18. (a) Experimental and predicted stress *vs.* strain response for high strain rate compression of non-basal textured zirconium. (b) Plots of accumulated twin volume fraction *vs.* strain for both twin modes. (c) Relative shear contribution of each deformation mechanism.

deformation modes allowed; in the clock-rolled material compression twinning is included, whereas in the cross-rolled material, compression twinning is replaced by <c+a> pyramidal slip. The contribution of the two twin modes can be somewhat misleading, since a twin of each type has a different twinning shear inherent to its formation. The 85° twin has a twinning shear of 0.167 while the 34° twin has a twinning shear of 0.63. This means that there could be a smaller fraction of 34° twins that collectively accommodate more shear than the 85° twins.

The advantage of modeling in this context is that it provides greater certainty that assumptions of homogeneous deformation can be met in these experiments. The choice of VPSC is appropriate because it uses local crystallographic information that is experimentally gathered to predict bulk response to loading. VPSC and other similar models often implicitly rely on dislocation and twin activity to achieve this end, which makes them unsuitable for explicit comparison with deformation processes directly observable in the TEM. To achieve this, dislocations need to be *directly* accounted for a model; a theory that does this is discussed in the next section.

Numerical Modeling

This section briefly summarizes two modeling approaches taken to address the plastic response at the mesoscale, the first applicable to determining effective behavior of polycrystalline materials, and the second to detailed mesoscale response of a single or a few crystals. These models have been described in previous progress reports (2004 Annual Report) and (2005 Annual Report).

A challenge for plasticity models, especially as progress is made towards a multiscale approach, is in the transition from single to polycrystalline materials. One of our goals is to incorporate slip transmission rules, at least in a phenomenological sense, into polycrystalline plasticity models. The approach has been to account for the grain boundary by considering bicrystal inclusions embedded in a Homogeneous Effective Medium (HEM). The plastic response of each grain in the bicrystal is modeled using a viscoplastic constitutive law, and equilibrium and compatibility conditions are enforced across the bicrystal boundary. The effective response of an aggregate of such bicrystal inclusions is obtained through homogenization using the ViscoPlastic Self-Consistent (VPSC) scheme [5]. The grain boundary

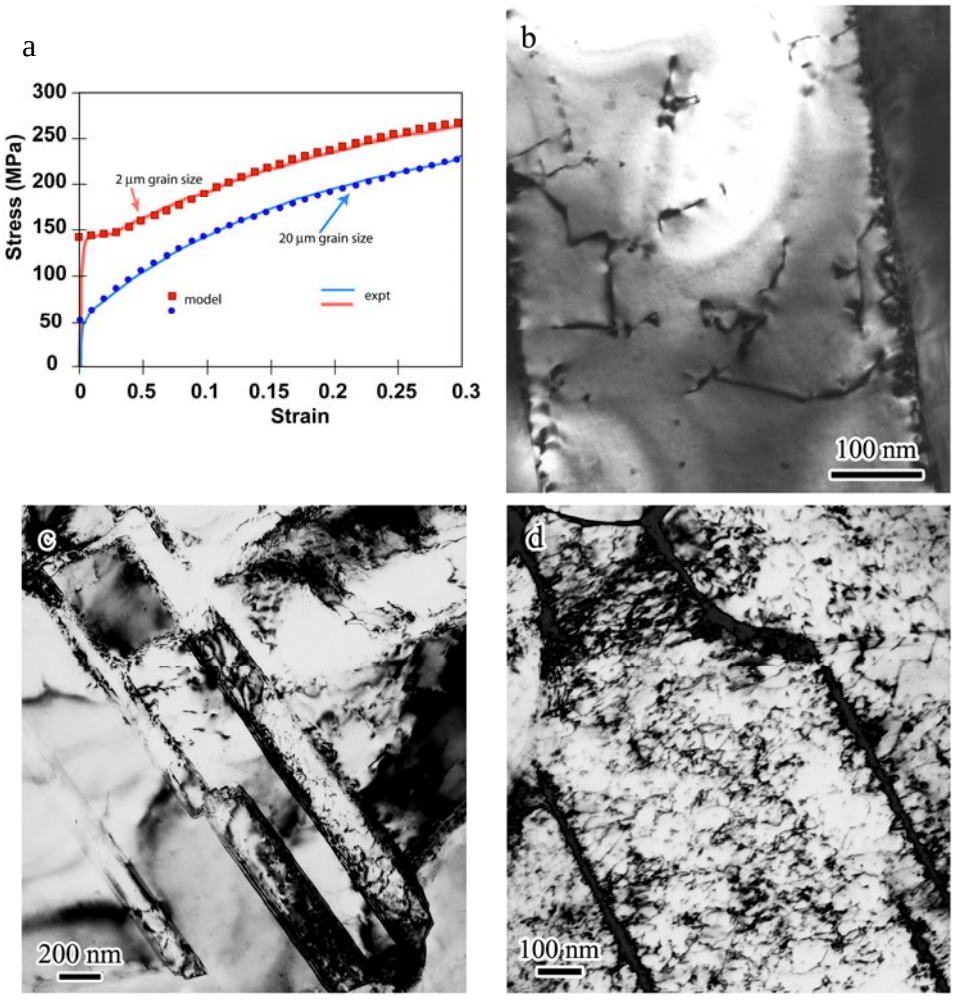

Figure 19. (a) stress-strain response of fine grained material, experimental and model (b) initial microstructure (c) microstructure at strain of 0.001% (d) microstructure at strain of 0.01%

orientation is accounted for by the bicrystal inclusion, and the local stress distribution through the viscoplastic constitutive law. In addition, in this *composite grain model*, the change in grain boundary energy is accounted for by development of latent hardening applied to slip systems that intersect the boundary and by using an effective "back stress" created as a result of residual dislocations at the boundary.

The effect of twin boundaries on the deformation of Silver, which was cold-rolled and subsequently annealed to produce twins, was studied both experimentally and numerically. The stress-strain response is characterized by a low proportional limit (about 20 MPa) followed by an elongated yield point at 140 MPa, followed by stage III hardening beyond a strain of a few percent (Figure 19a). The microstructure prior to deformation is dominated by annealing twins within the 2 **µ**m grains, and dislocation half-loops are seen emerging from the twin boundaries; the dislocation density elsewhere in the specimen is low (Figure 19b). After deformation, microstructure at the proportional limit (Figure 19c) and the yield point (Figure 19d) consists of a high dislocation density within and outside the annealing twins; these observations imply that

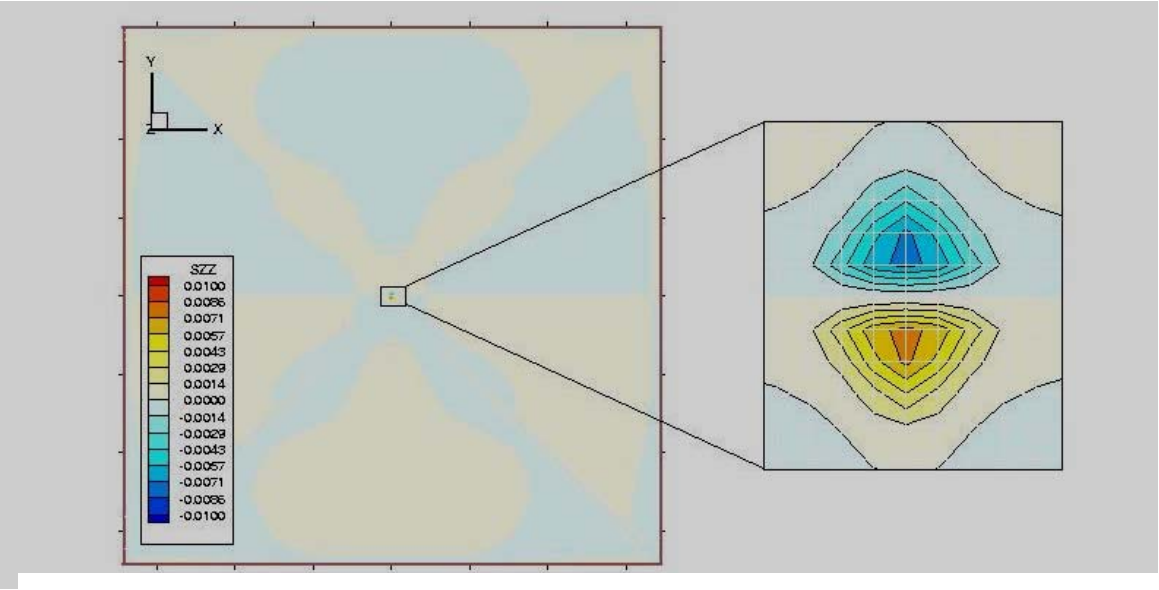

Figure 20. Stress field of a single edge dislocation determined using FDM.

the twin boundaries were sources of dislocations, in addition to being barriers to dislocation motion. Motivated by these experimental observations, evolution equations for mobile and forest dislocation densities [15] were introduced into the composite grain model, where the two phases in each inclusion were separated by a $\Sigma 3$ boundary. It is clear from Figure 19a that an essential feature of the macroscopic response, the yield point elongation, is captured by the composite grain model. This model has also been successfully applied to the study of texture development in Cu/Nb multilayered materials [16].

Another complementary approach based on Field Dislocation Mechanics (FDM) [17, 18] and crystal plasticity is constructed to model the collective behavior of dislocations. This detailed approach is computationally intensive, but is capable of directly modeling dislocation interaction and transport. The basic idea behind FDM is that dislocations have a stress field which, along with the stress field due to the traction and displacement boundary conditions, drives their motion and results in permanent deformation and residual stress in the material. This continuum theory provides for the calculation of lattice distortion, stress, dislocation density evolution and slip plastic strain. In the combined model, FDM is used to model Geometrically Necessary Dislocations (GND) and crystal plasticity is used to model Statistically Stored Dislocations (SSD). GND have a long-range stress field and contribute to plastic flow, while SSD only contribute to plastic flow. There is a two-way coupling between FDM and crystal plasticity: non-uniform plastic flow of SSD creates a source term for GND, while GND are forest obstacles to the flow of SSD. The governing equations, together with their numerical formulation, were described in (2005 Annual Report). Further details can be found in [19,20].

A few preliminary applications are presented below, illustrating the scope of the theory. The first category of applications deals with the calculation of the stress field of dislocations. In this case, FDM reduces to the elastic theory of continuously distributed dislocations [21]. The stress field of a single edge dislocation (modeled as a density) is shown in Figure 20. An interesting case, where dislocation arrangements are such that there is no long-range stress field (zero stress equivalent field [22]) is shown in Figure 21. Here the dislocations are arranged to

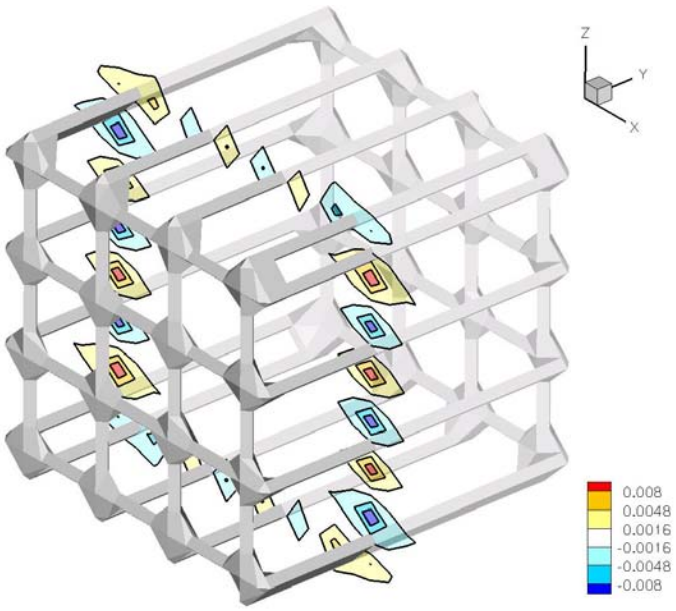

Figure 21. Zero stress equivalent field for a crossgrid of screw dislocation densities.

form loops in perpendicular planes (crossgrid of screw dislocation densities). Another example which deals with the motion of dislocations (under an applied stress field and their own interaction) is illustrated in Figure 22. A block with an initial assembly of positive and negative edge dislocations is subjected to simple shear. The dislocations glide under the applied stress field, disperse due to self-stress and exit the domain, after which the response is elastic. The formation of slip steps where the dislocations exit can be noted.

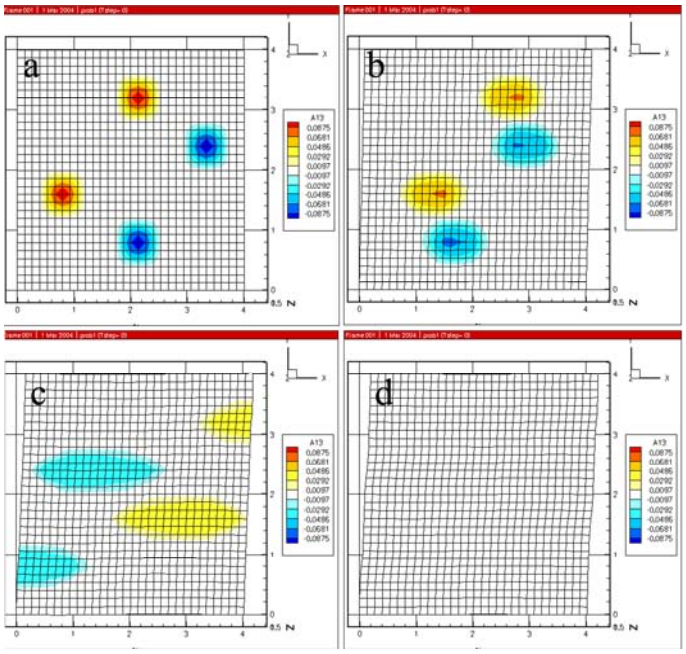

Figure 22. Dispersion of edge dislocation densities during deformation

`

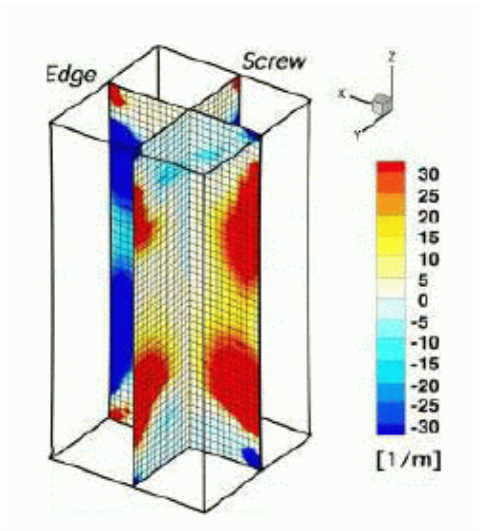

Figure 23. Mobile components of GND density.

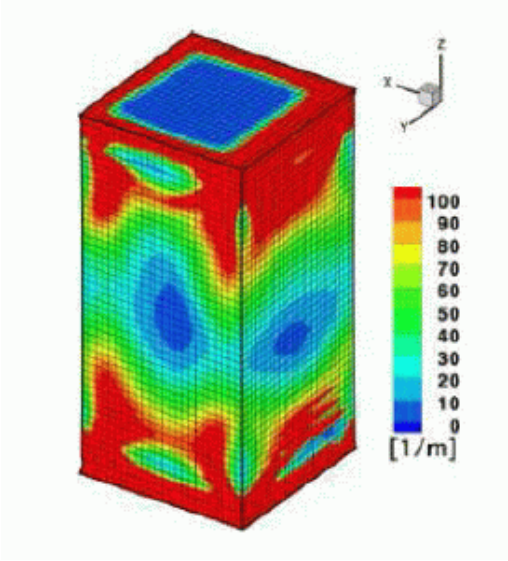

Figure 24. Magnitude of GND.

A Frank-Read source simulation was presented in (2005 Annual Report); FDM can model growth in dislocation density due to kinematics and annihilation, without the prescription of additional source terms. A link with the Hamilton-Jacobi equations was established in [19].

Next, we will consider applying the combined model to incipient pattern formation. A specimen 3 microns in length is subjected to tension with the lateral edges constrained on the top and bottom faces. There is no initial GND, and the domain is uniformly initialized with SSD. The crystal plasticity slip planes are oriented for single slip condition. The effect of the laterally constrained edges is to introduce an inhomogeneity in the stress field (and hence plastic strain rate), which triggers the formation of GND. The mobile component and magnitude of GND are shown in Figures 23 and 24 respectively -- the screw and edge dislocation density have opposing sign on opposite sides of the specimen, giving the impression of a loop structure.

Because of high anisotropy due to limited slip on non-basal systems, ice presents an excellent model material for studying the interplay between internal stress and excess dislocation density. Such study provides insight into the behavior of other HCP materials (e.g. Zr), where quantifying the effects of internal stress developed in the deformation of basal textured material presents a difficult task. The combined model has also been applied to study torsional creep in ice [23]. The softening behavior in primary creep in torsion observed in experiments has been reproduced, and interpreted in terms of the dynamics of excess screw dislocations gliding on basal planes (Figure 25).

In summary, the strength of this model lies in the fact that dislocations and their interaction are accounted for explicitly, on sound physical bases. This results in a natural way of modeling size effects on flow stress, kinematic hardening (back-stress), formation of structure, and dislocation interaction with boundaries, all of which are currently under investigation.

FCC Conclusions

1. Nano-indentation measurements of the hardness on and near a grain boundary do not provide a good measure of the slip transmissibility factor.

`

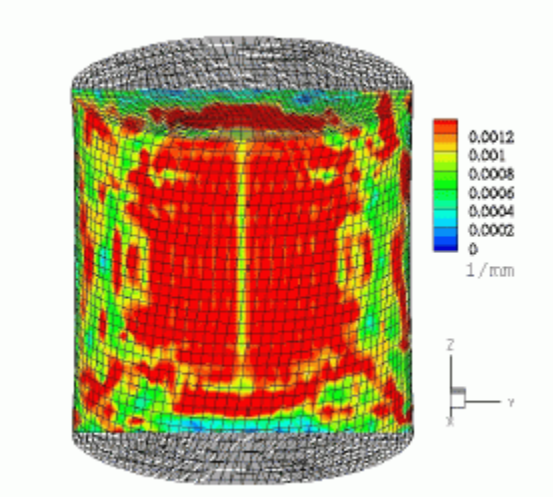

Figure 25. Pileup of screw density on basal planes in torsion of ice

2. Perfect and partial dislocations can be emitted from the same region of a twin boundary in response to local stress conditions within the twin boundary plane. This occurs in a material with a low stacking-fault energy.
3. Deformation twins can act as barriers to dislocation slip until the internal strain reaches a level to activate dislocations sources within the twin boundary.
4. Deformation twins are observed to nucleate from planar slip bands in a low stacking-fault energy nitrogen-strengthened austenitic steel alloy.
5. Long bands of deformation twins are formed from the overlap of shorter twin segments suggesting a mechanism for how deformation twins can seemingly propagate through dense regions of pre-existing defects.
6. The tamped laser ablation technique allows for deforming sample materials at high strain rates, but to relatively low levels of strain, facilitating investigation of twin nucleation mechanisms.

HCP Conclusions

1. Tensile twinning is energetically favorable for non-basal textured polycrystals.
2. Both slip and deformation twinning are active in basal and non-basal SHPB compression tests, with the amount of deformation twinning strongly dependent on the starting texture.
3. Nearly complete energy dissipation is observed for non-basal compression, and there is the appearance of incomplete dissipation for basal compression.
4. Localization in basal-textured specimens invalidates β measurements, and can explain the apparent energy storage.
5. Modeling of non-basal grains shows a sufficient condition for bulk homogeneous deformation at the length scale of several hundred microns.
6. Non-basal compression results are similar to results from collaborators at LANL, while basal compression results show different mechanisms.

Modeling Conclusions

1. A composite grain model based on homogenization theory was developed for the transition from single to polycrystalline mechanics, and successfully applied to the study of texture development in Cu/Nb multilayer, and prediction of stress-strain response of twinned silver.
2. A model based on continuum dislocation mechanics is being developed, for modeling interaction of dislocations with boundaries, structure formation, and dislocation-solute interaction. This more fundamental approach can be used to gain insight into deformation mechanisms at the mesoscale, which can then be incorporated in a phenomenological sense into macroscopic models such as the composite grain model.

References

[1] Lee, T.C., I.M. Robertson, H.K. Birnbaum, *Phil Mag A*, 1990, vol. 62, p. 131.
[2] Lee, T.C., I.M. Robertson, H.K. Birnbaum, *Metall. Trans. A*, 1990, vol. 21A, p. 2437.
[3] Padilla, H. A., C.D. Smith, J. Lambros, A.J. Beaudoin and I.M. Robertson, submitted to *Met Trans A*, 2007
[4] Molinari, A., G.R. Canova and S. Azhi: *Acta Metall*, 1987, vol. 35, pp. 2983-2994
[5] Lebensohn, R.A. and C.N. Tomé: *Acta Metall. et Mater.*, 1993, vol. 41, pp. 2611-2624
[6] Kaschner, G.C. and G.T. Gray III: *Metal.Mater. Trans. A*, 2000, vol. 31A, pp. 1997-2003
[7] McCabe, R.J., E.K. Cerrata, A. Misra, G.C. Kaschner, and C.N. Tomé: *Philisophical Magazine*, 2006, vol. 86, p.3595-3611
[8] Mason, T.A., J.F. Bingert, G.C. Kaschner, S.I. Wright, and R.J. Larsen: *Metallurgical Transactions A*, Series A, 2002, vol. 33A, pp. 949
[9] Akhtar, A.: *Journal of Nuclear Materials*, 1973, vol. 47, pp. 79-86
[10] Farren, W.S. and G.I. Taylor: *Pro. Royal Soc. London*, 1925, Series A, vol. 107, pp. 422-451
[11] Bever, M.B., D.L. Holt and A.L. Titchener: *Progress in Materials Science*, 1973, vol. 17, p. 192
[12] Mason, J.J., A.J. Rosakis and G. Ravichandran: *Mechanics of Materials*, 1994, vol. 17, pp. 135-145
[13] Subhash, G., G. Ravichandran, and B.J. Pletka: *Metall. Trans. A*, Series A, 1997, vol. 28A, pp. 1479-1487
[14] Tomé, C.N., P.J. Maudlin, R.A. Lebensohn and G.C. Kaschner: *Acta Mate.*, 2001, vol. 49, pp. 3085-3096
[15] Kubin, L.P., and Y. Estrin: *Acta Metall.*, 1990, vol. 38, p 697.
[16] Al-Fadhalah, K., C.N. Tome, A.J. Beaudoin, I.M. Robertson, J.P. Hirth and A. Misra: *Phil. Ma*, 2005, vol. 85, pp 1419-1440.
[17] Acharya, A.: *J. Mech. Phys. Solids*, 2001, vol. 49, pp 761-784.
[18] Acharya, A. and A. Roy: *J. Mech. Phys. Solids*, 2006, vol. 54, pp 1687-1710.
[19] Varadhan, S.N., A.J. Beaudoin, A. Acharya and C. Fressengeas: Modelling and Simulation in Materials Science and Engineering, 2006, vol. 14, pp 1245-1270.
[20] Varadhan, S.N., A.J. Beaudoin and C. Fressengeas: Proceedings of International Congress on Statistical Mechanics and Related Instabilities, 2005, PoS(SMPRI2005)004.
[21] Willis J R (1967), "Second-order effects of dislocations in anisotropic crystals," *International Journal of Engineering Sciences*, vol. 5, pp 171 - 190.

[22] Head, A.K., S.D. Howison, J.R. Ockendon and S.P. Tighe: Society of Industrial and Applied Mathematics Review, 1993, vol. 35, pp 580-609.
[23] Taupin, V., S.N. Varadhan, J. Chevy, C. Fressengeas, A.J. Beaudoin, M. Montagnat and P. Duval: Physical Review Letters, 2007 (submitted).